Electronic Supplementary Material (ESI) for Nanoscale Advances.

Synthesis of α”-$Fe_{16}N_2$ ribbons with porous structure

Jinming Liu[1], Guannan Guo[1], Fan Zhang[1,2], Yiming Wu[2], Bin Ma[1], Jian-Ping Wang[1,2,*]

[1]*Department of Electrical and Computer Engineering, University of Minnesota, 200 Union Street SE Minneapolis, MN, 55455*

[2]*Niron Magnetics, 650 Taft St NE #400, Minneapolis, MN, 55413*

*Author to whom the correspondence should be addressed. Email: jpwang@umn.edu

1. Schematic flow chart of the microstructure change of the ribbon samples

For the raw ribbon sample made by a melt spinning system, the grain size is small. The grain growth of the quenched ribbon sample was expected due to the high temperature heat treatment up to 930 °C. Based on the Fe-N binary phase diagram,[1] body-centered cubic (bcc) Fe will transform into the face-centered cubic (fcc) Fe at the temperature around 910 °C and new grain boundaries could be generated due to the phase transformation happens around this temperature. The grain boundaries obtained from the thermal treatment would help enhance the nitridation efficiency dramatically. Then, the hydrogen reduction was processed to make the ribbon sample ready of the low-temperature nitriding. During this step, the ribbon showed foam-like porous structure. And then the nitridation processed at relatively low temperature 160 °C. There was no obvious grain growth during the low-temperature nitriding process, and the microstructure of the nitride ribbon sample was similar to that of the reduced one.

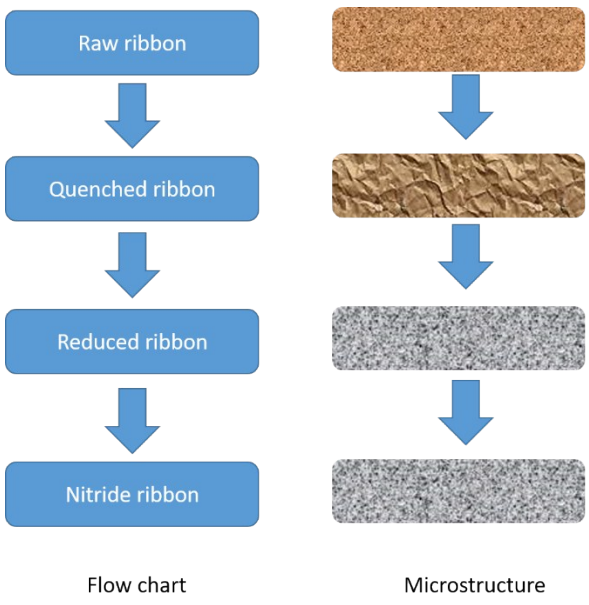

Figure S1. Flow chart of the sample preparation and the schematic drawing of the microstructures of the ribbon sample at each step

2. Magnetic properties of FeCuB ribbons

In-plane (IP) and out-of-plane (OP) magnetic hysteresis loops were measured by vibrating sample magnetometry (VSM) to characterize the magnetic properties of these ribbon samples (raw ribbon, quenched sample, reduced sample). The coercivity (H_c) of the raw ribbon was ~50 Oe. After the heat treatment at 930 ^oC and quenching the sample to room temperature distilled water, the H_c of the quenched sample doubled which was due to the iron oxide formed during the quenching process. The quenched sample was reduced by hydrogen at 350 ^oC and the H_c was decreased. In these loops we could also see the change of saturation magnetization (M_s) for the raw ribbon, quenched sample and reduced sample. The M_s of the raw ribbon is ~190 emu/g which was smaller than that of bcc Fe (~220 emu/g) since Cu and B were added into the raw ribbon. The quenched sample had M_s as low as 30 emu/g because of the oxidation which was consistent with the XRD patterns shown in the manuscript. M_s of the hydrogen-reduced sample was around 30 emu/g smaller than the raw ribbon. The reduced M_s was due to the born oxide phases which could not be reduced by hydrogen at 350 ^oC. The OP loops of the raw ribbon, quenched sample, and reduced sample showed higher saturation field than that of the IP case. The hysteresis loops of the raw ribbon sample, quenched ribbon sample, and reduced ribbon sample were shown in figure S2 (a) and (b). The M_s and H_c of ribbon samples at each step were summarized in figure S3 using the data of IP loops. The M_s of the ribbon sample decreased after quenching step due to the sample oxidation, recovered again after the hydrogen reduction, and dropped a little bit after nitridation due to the sample oxidation. The Hc of ribbon samples were smaller than 100 Oe for the raw ribbon sample, quenched ribbon sample, and reduced ribbon sample because there were no hard magnetic

phases in the samples. After nitridation, the H_c increased dramatically due to the formation of the hard magnetic phase α"-$Fe_{16}N_2$.

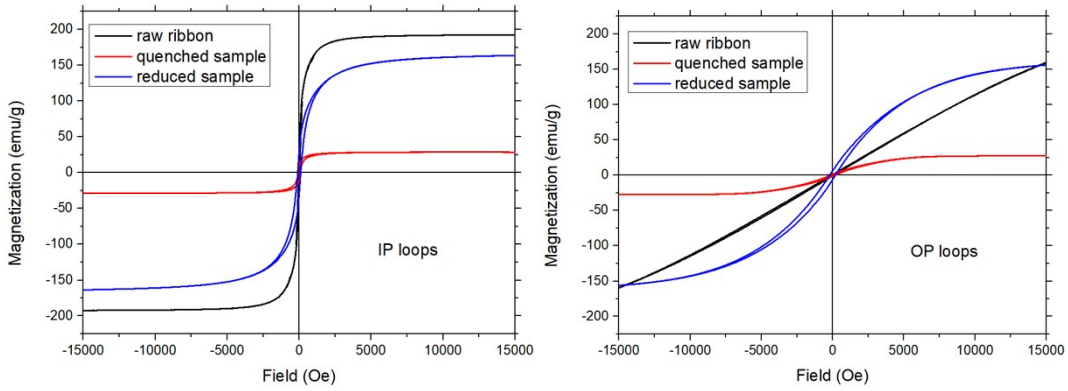

Figrue S2. Hysteresis loops of raw ribbon, quenched sample, and reduced sample, (a) IP loops, and (b) OP loops.

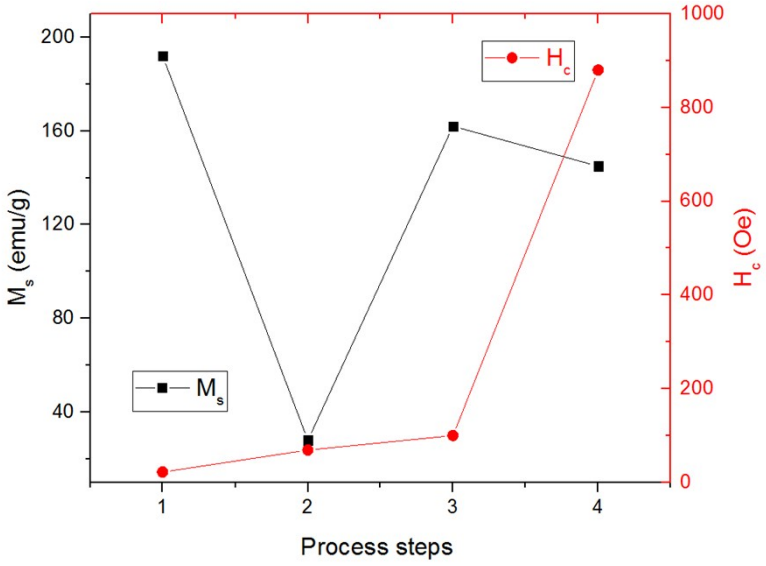

Figrue S3. M_s and H_c of the ribbon samples (IP loop data) at each step: 1 raw ribbon sample; 2 queched ribbon sample; 3 reduced ribbon sample; 4 nitride ribbon sample.

3. Effective magnertic anisotropy estimation by the law of approach to saturation

The magnetization curve could be expressed as the equation below. [2,3]

$$M = M_s\left(1 - \frac{a}{H} - \frac{b}{H^2} - \frac{c}{H^3} - \ldots\right) + \chi_p H$$

where M_s is the saturation magentization, *a, b,* and *c* are constant coefficients, and only b relates with the magnetocrystalline anisotropy. For polycrystalline materials with uniaxial anisotropy, the anisotropy constant K_u could be calculated as

$$b = \frac{4}{15} \times \frac{K_u^2}{M_s^2}$$ [3]

The fitting curves were shown in figure S2. The anistropy constant could be calculated as $K_u = \frac{\sqrt{15b}}{2} M_s$. The theoretical density of α"-$Fe_{16}N_2$ is around 7.46 g/cm^3. The saturation magentization value was derived by subtracting the contribution of born oxide. Therefore, the K_u is around 3.6×10^6 erg/cm^3.

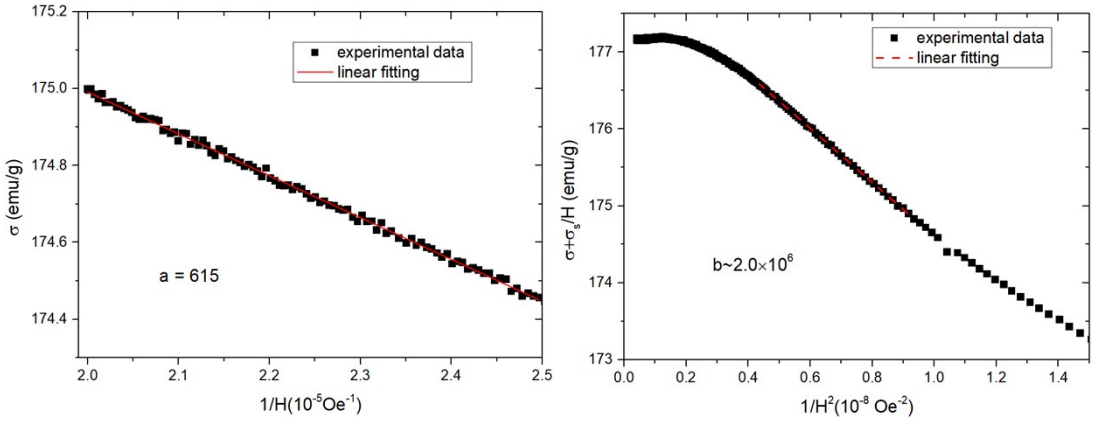

Figrue S4. Fitting data based on the law of approach to saturation. The σ here was the specific magnetization and σ_s is the saturation specific satruation magnetization.

References:

1 E. H. D. M. van Voorthuysen, D. O. Boerma and N. C. Chechenin, *Metall. Mater. Trans. A*, 2002, **33**, 2593–2598.

2 J. P. Wang, D. H. Han, H. L. Luo, Q. X. Lu and Y. W. Sun, *Appl. Phys. A Mater. Sci. Process.*, 1995, **61**, 407–413.

3 K. Ho, X. Xiong, J. Zhi and L. Cheng, *J. Appl. Phys.*, 1993, **74**, 6788–6790.